Surface Enhanced Raman Scattering of Crystal Violet

Jones, R. R.[a,b], Batten, T.[c], Smith, B.[c], Silhanek, A.V.[d], Wolveron, D.[b,a], Valev, V. K.[a,b]
[a]Centre for Photonics and Photonic Materials, University of Bath, Bath, BA2 7AY, United Kingdom; [b]Centre for Nanoscience and Nanotechnology, University of Bath, Bath, BA2 7AY, United Kingdom; [c]Renishaw Plc, Wotton-under-Edge, UK; [d]Experimental Physics of Nanostructured Materials, Q-MAT, CESAM, Université de Liège, Sart Tilman B-4000, Belgium

ABSTRACT

Despite the ubiquity of Raman spectroscopy, fluorescence, poor signal strength and photobleaching pose a significant challenge to researchers in the biomedical field. Here, we demonstrate a 17-fold signal enhancement in Raman spectra of crystal violet via surface-enhanced Raman scattering (SERS). The SERS substrate was fabricated by electron beam lithography (EBL); the nanostructured surface was an array of G-shaped elements made of Au on SiO_2/Si. In addition to the SERS spectra, finite-difference time-domain simulations were performed to illustrate the distribution of electric-field hot-spots on the SERS substrate. The electric-field hot-spots were prominent at the vertices and edges of the nanostructured G-shaped motifs. The results presented here demonstrate that EBL is a high-end choice for SERS substrate fabrication that opens the way for more complex Raman spectroscopies, for instance involving nonlinear optics or chiral analytes.

Keywords: Surface enhanced Raman scattering, crystal violet, finite-difference time-domain simulation, electron beam lithography

1. INTRODUCTION

Raman scattering spectroscopy is a versatile technique that exploits the inelastic scattering of light to characterize and identify chemicals and materials based on their quantized vibrational energy levels[1–4]. When light inelastically scatters via a light-matter interaction, the light can lose energy (Stokes scattering) by increasing the energy of vibration (or rotational-vibration) of the scattering analyte. If, however, the analyte is initially in an excited state of vibrational energy, the light can gain energy via the scattering event leaving the analyte in a lower energy state. Most instruments observe the Stokes Raman shift in wavelength of the scattered light meaning that the observed wavelength is larger than the incident light. The observed Raman shifts are typically quantized according to the quantization of vibrational energy levels in the scattering material and are subject to selection rules[5]. Hence, crystals and molecules can be identified by their unique Raman spectrum of distinct peaks.

Raman spectroscopy is particularly attractive to biologists as it is a chemically selective hyperspectral imaging technique that seldom requires pretreatment of the specimen with molecular tags. These pretreatment techniques of tissues invariably alter the metabolic processes of the cells[6,7]. Despite these advantages, Raman spectroscopy can be challenging with certain types of samples due to fluorescence or photobleaching. Sometimes, these effects can be mitigated by increasing the wavelength of the incident light or by algorithmically removing the background fluorescence[8]. However, Raman scattering is an inherently weak effect with only 1 in 10^8 photons undergoing spontaneous Raman scattering[9]. Hence, researchers often employ plasmonic effects to enhance the Raman signal.

Raman spectroscopy has become a useful tool for characterizing a variety of materials, such as 2D materials (including graphene[10–12] and transition metal dichalcogenides[13–15]). Raman spectroscopy can help establish the number of monolayers[11,14,16,17], interlayer breathing and shear modes[18], in-plane anisotropy[19], doping[20–22], disorder[12,23–25], thermal conductivity[13], strain[26] and phonon modes[27–29].

Surface enhanced Raman scattering (SERS) was first observed in 1974 when Fleischmann et al. noticed a significant increase in the Raman signal of pyridine on a roughened silver electrode[30]. SERS can be achieved using various forms of nanostructured materials, such as plasmonic nanoparticles. Surface plasmons are coherent oscillations of the surface electrons in metals that can be driven by visible light[31]. Numerous theoretical models have been proposed in order to achieve such tuning[32,33]. Nanoparticle aggregates are a common method for SERS but the consistency of aggregation, and hence the homogeneity of enhancement, can be challenging[34–38]. Electron beam lithography is an exquisitely precise method for producing SERS substrates with homogeneous hot-spots of SERS[39,40]. The G-shaped nanoarrays have been the subject of numerous experimental studies, especially using second harmonic generation[41,42] – an interface-sensitive technique[43,44] whose efficiency scales as the fourth power of the optical near-fields, similarly to the enhancement factor of SERS[45,46].

Here, we demonstrate SERS using plasmonic G-shaped nanostructures fabricated from Au on a SiO_2/Si substrate using electron beam lithography as detailed in refs[47]. Crystal violet (CV) is used as the analyte as it constitutes an excellent reference, with a distinct and well known Raman spectrum[48].

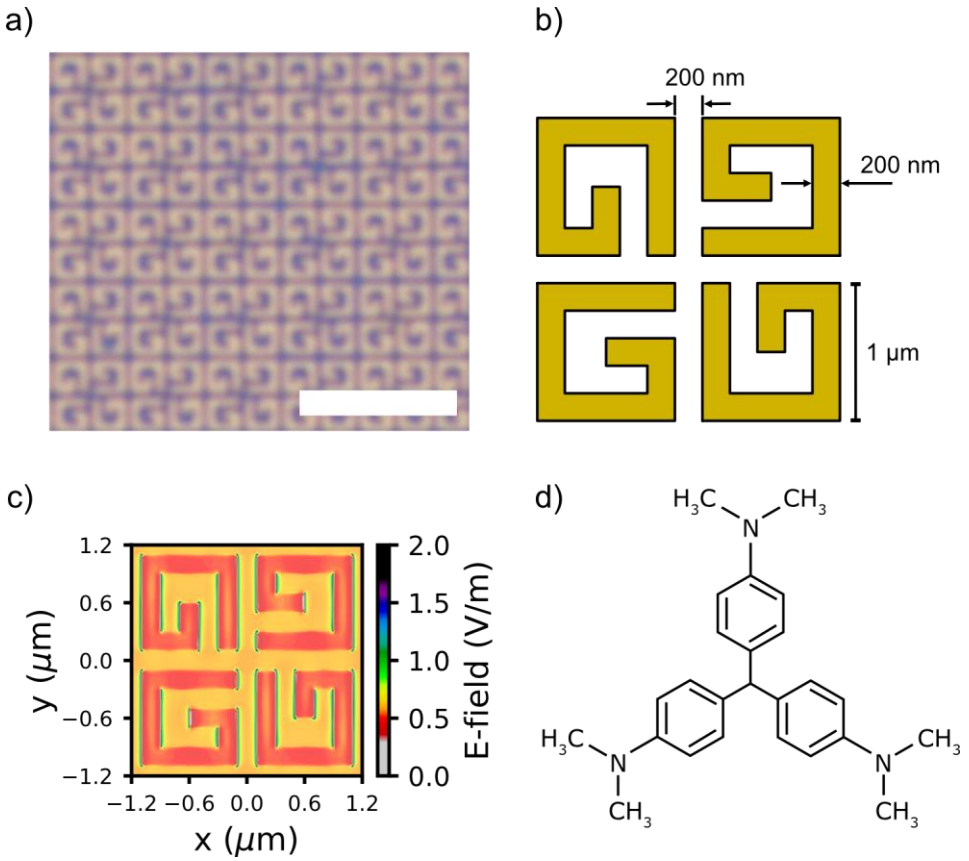

Figure 1. a) bright field microscope image of the G-shaped SERS substrate; scale bar 5 µm. b) schematic of the geometry of the nanostructured SERS substrate fabricated as per refs[47] c) simulation results of the electric-field distribution at 532 nm taken 1 nm above the SERS substrate. d) molecular structure of crystal violet.

2. EXPERIMENTAL PROTOCOL

Raman spectra of CV were acquired using a Renishaw InVia Raman microscope. A continuous wave laser (50 mW Cobolt RL532-08) was used to provide a narrow bandwidth light source at 532 nm on the sample. The spectrometer used a 1800 lines/mm grating blazed for 532 nm. The incident radiation and epi-scattered light were focused through an N-plan 50× objective with a numerical aperture of 0.75. Unless otherwise stated, spectra were averaged from a square grid of 25 uniformly distributed points (1 µm apart for CV on SERS and 5 µm apart for CV on Si to account for the increased inhomogeneity in CV distribution on bare Si). At each point on the grid, the spectrum acquisition was 10 seconds with

the spectrometer slit width set to 60 µm wide. The spectral resolution of the spectrometer is 0.3 cm^{-1}. The fluorescence background was removed using a polynomial fit algorithm in the Renishaw WiRE software.

The SERS substrate was fabricated on a Silicon substrate with a thermally grown 200 nm SiO_2 surface layer. A double polymethyle metacrylate-methyl metacrylate resist layer was used to cover the substrate. The G-shaped nanostructures were then created by electron beam lithography. A 25 nm layer of Au was deposited by evaporation using a DC sputtering system[47]. The resist was then removed by a 'lift-off' procedure. Figure 2 a) shows a bright field microscope image of the G-shaped nanostructured SERS substrate taken using a 100× objective. The geometry of the unit cell with the associated dimensions is shown in Figure 3 b); the unit cell comprised of four such motifs in a four-fold tetrad. The array of Au nanostructures covered an area of 2.5 mm × 2.5 mm on the Si substrate. Hence, the enhancement of the Raman signal from CV on the SERS part of the sample was compared to measurements of CV on the clean Si area of the sample.

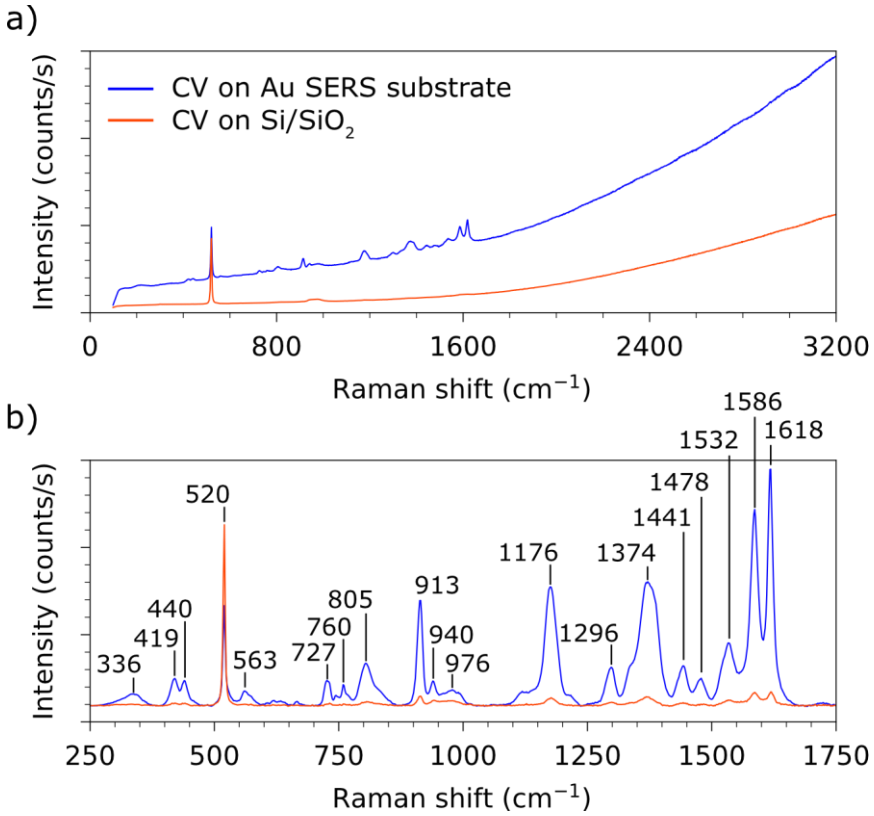

Figure 4. Raman spectra of crystal violet on the SERS substrate and on silicon using 532 nm incident excitation. a) full range of Raman shifts taken at a single point with 100% of the available laser power for 10 seconds. b) spectral region of interest with fluorescence background removed taken from a uniform 5 × 5-point grid (25 points in total) with a 10 second acquisition per point and averaged; the laser power was attenuated to 10% using neutral density filters. The sample points in the map had a granularity of 1 µm on the SERS substrate and 5 µm on the silicon substrate to account for increased inhomogeneity in the distribution of CV on bare Si.

Finite-difference time-domain simulations can be performed with a variety of Maxwell equations solvers, such as MAGMAS[49,50], Lumerical[51], MEEP[52], RSoft's DiffractMOD[53], etc. We performed simulations in ANSYS™ Lumerical to illustrate the concentration of electric field 'hot-spots' at the vertices of the G-shaped structures. The geometry of the simulation was based on that shown in Figure 5 b). Periodic boundary conditions were imposed around the edges of the unit cell to simulate an infinite array of unit cells. The Si substrate model was a 500 nm thick slab of Si based on Palik material model[54]. The G-shaped unit cell was modelled in Autodesk Inventor and imported into Lumerical with a CRC material model[55]. A plane wave source was introduced from 1 µm above the surface with a wavelength range of 0.2 to 1.8 µm. The void above the plane wave source extended by an additional 1 µm. Perfectly

matched layer boundary conditions were applied to the top and bottom plane of the simulation domain. Hence, the simulation perceived the Si substrate to be infinite in extent. Figure 6 c) shows the electric field distribution at 532 nm taken in the plane 1 nm above the surface of the Au G-shaped nanostructures. The electric field hot-spots are clearly concentrated at the edges and vertices of the G-shaped motifs as expected.

A 0.3 mM solution of CV in ethanol was drop-casted onto the SERS subsrate and allowed to evaporate in air. Because CV has three amino groups, it bonds to the Au surface and the effect of liquid tension during the evaporation of ethanol is minimized. Figure 7 d) shows a schematic of the organic molecule that is used for our demonstraton of SERS; it has also been used in surface enhanced hyper-Raman scattering experiments[56].

3. RESULTS AND DISCUSSION

Figure 8 a) shows a spectrum of CV on the Au SERS substrate (blue) and on bare Si (red). These spectra (Fig. 9a) were acquired using 100% of the available laser power at a single point on the sample with an acquisition time of 10 seconds. The presence of fluorescence is evident and was subsequently removed using a polynomial fit algorithm in the Renishaw WiRE software. The distinct peak at 520 cm^{-1} corresponds to the Raman peak of Si.

Table 1. Raman peaks of crystal violet identified on the SERS substrates with associated band assignments measured using 532 nm excitation; band assignment taken from ref.[48].

Raman shift (cm^{-1})	Band assignment
727, 760, 805	C-H out of plane bending
913, 940, 976	Ring skeletal vibrations
1176	C-H in plane bending
1374	N-phenyl stretching
1532, 1586, 1618	C-C stretching

Figure 10 b) presents the spectra of CV measured on the SERS surface and on the Si surface in the finite range of Raman shifts of interest. The fluorescence background has been removed using the method stated above. Again, the Raman peak of Si at 520 cm^{-1} is observed. The prominent Raman peaks associated with CV are labelled and identified. The band assignments are presented in Table 1 and are in good agreement with refs[48,57]. The enhancement of the signal on the SERS sample is approximately 17× that of the measurements taken from CV on the Si surface. Hence, we demonstrate that these samples, fabricated using electron beam lithography, are excellent SERS substrates with good homogeneity.

4. CONCLUSIONS

We have demonstrated a 17-fold signal enhancement of Raman scattering spectra in crystal violet using a G-shaped Au nanostructured SERS substrate relative to CV on Si wafer. Finite-difference time-domain simulations revealed that the electric field enhancement was most concentrated in the vicinity of the edges and vertices of the nanostructured motifs. EBL is a rather costly and time-consuming method, with limited potential for scaling up production, especially in the case of large area SERS substrates. However, the commercial availability of SERS substrates with homogeneous and reproducible enhancement in Raman scattering is also limited. EBL provides excellent nanoscale precision and design freedom that can be greatly beneficial for tailoring the SERS substrate to a particular analyte. The SERS enhancement can be further augmented by tuning the resonance wavelength of the nanoparticles to that of the incident laser. Nanostructures with a chiral design[58], such as the G-shaped nanoarrays, could next be used for chiral optical SERS investigations. Moreover, as they have well-known nonlinear optical conversion properties, these nanoarrays open the way for surface enhanced hyper-Raman scattering studies. Therefore, our work paves the way for SERS-based investigations of chiral organic molecules, such as pesticides and pharmaceuticals in the environment. Moreover, SERS find applications in the detection of explosives/chemical weapons[59], unmodified DNA[60], and pathogens[61].

ACKNOWLEDGMENTS

V.K.V. acknowledges support from the Royal Society through the University Research Fellowships and the Royal Society grants RGF\EA\180228, and funding from the Engineering and Physical Sciences Research Council (EPSRC) grant EP/T001046/1. D.W. acknowledges support from the EPSRC with Renishaw Plc 2019 iCASE award EP/T517495/1.

SUPPORTING INFORMATION

All data supporting this study are openly available from the University of Bath data archive at https://doi.org/10.15125/BATH-00991.

REFERENCES

[1] Jones, R. R., Hooper, D. C., Zhang, L., Wolverson, D. and Valev, V. K., "Raman Techniques: Fundamentals and Frontiers," Nanoscale Res. Lett. **14**(1) (2019).

[2] Smekal, A., "Zur quantentheorie der dispersion," Naturwissenschaften **11**(43), 873–875 (1923).

[3] Raman, C. V. and Krishnan, K. S., "A new type of secondary radiation," Nature **121**(3048), 501–502 (1928).

[4] Das, R. S. and Agrawal, Y. K., "Raman spectroscopy: Recent advancements, techniques and applications," Vib. Spectrosc. **57**(2), 163–176 (2011).

[5] Long, D. A., [The Raman effect], John Wiley & Sons, Ltd, Chichester, UK (2002).

[6] Hellerer, T., Axäng, C., Brackmann, C., Hillertz, P., Pilon, M. and Enejder, A., "Monitoring of lipid storage in Caenorhabditis elegans using coherent anti-Stokes Raman scattering (CARS) microscopy," Proc. Natl. Acad. Sci. **104**(37), 14658 LP – 14663 (2007).

[7] Maier, O., Oberle, V. and Hoekstra, D., "Fluorescent lipid probes: some properties and applications (a review)," Chem. Phys. Lipids **116**(1), 3–18 (2002).

[8] Bocklitz, T., Walter, A., Hartmann, K., Rösch, P. and Popp, J., "How to pre-process Raman spectra for reliable and stable models?," Anal. Chim. Acta **704**(1–2), 47–56 (2011).

[9] Bowley, H. J., Gardiner, D. J., Gerrard, D. L., Grave, P. R., Louden, J. D. and Turrell, G., [Practical Raman spectroscopy], Springer Berlin Heidelberg, Berlin, Heidelberg (1989).

[10] Venezuela, P., Lazzeri, M. and Mauri, F., "Theory of double-resonant Raman spectra in graphene: Intensity and line shape of defect-induced and two-phonon bands," Phys. Rev. B **84**(3), 035433 (2011).

[11] Malard, L. M., Pimenta, M. A., Dresselhaus, G. and Dresselhaus, M. S., "Raman spectroscopy in graphene," Phys. Rep. **473**(5–6), 51–87 (2009).

[12] Pimenta, M. A., Dresselhaus, G., Dresselhaus, M. S., Cançado, L. G., Jorio, A. and Saito, R., "Studying disorder in graphite-based systems by Raman spectroscopy," Phys. Chem. Chem. Phys. **9**(11), 1276–1290 (2007).

[13] Yan, R., Simpson, J. R., Bertolazzi, S., Brivio, J., Watson, M., Wu, X., Kis, A., Luo, T., Hight Walker, A. R. and Xing, H. G., "Thermal conductivity of monolayer molybdenum disulfide obtained from temperature-dependent Raman spectroscopy," ACS Nano **8**(1), 986–993 (2014).

[14] Lee, C., Yan, H., Brus, L. E., Heinz, T. F., Hone, J. and Ryu, S., "Anomalous lattice vibrations of single- and few-layer MoS2," ACS Nano **4**(5), 2695–2700 (2010).

[15] Verble, J. L., Wietling, T. J. and Reed, P. R., "Rigid-layer lattice vibrations and Van der Waals bonding in hexagonal MoS2," Solid State Commun. **11**(8), 941–944 (1972).

[16] Gupta, A., Chen, G., Joshi, P., Tadigadapa, S. and Eklund., "Raman scattering from high-frequency phonons in supported n-graphene layer films," Nano Lett. **6**(12), 2667–2673 (2006).

[17] Ferrari, A. C., Meyer, J. C., Scardaci, V., Casiraghi, C., Lazzeri, M., Mauri, F., Piscanec, S., Jiang, D., Novoselov, K. S., Roth, S. and Geim, A. K., "Raman spectrum of graphene and graphene layers," Phys. Rev. Lett. **97**(18), 187401 (2006).

[18] Zhao, Y., Luo, X., Li, H., Zhang, J., Araujo, P. T., Gan, C. K., Wu, J., Zhang, H., Quek, S. Y., Dresselhaus, M. S. and Xiong, Q., "Interlayer breathing and shear modes in few-trilayer MoS2 and WSe2," Nano Lett. **13**(3), 1007–1015 (2013).

[19] Chenet, D. A., Aslan, O. B., Huang, P. Y., Fan, C., van der Zande, A. M., Heinz, T. F. and Hone, J. C., "In-plane anisotropy in mono- and few-layer ReS2 probed by Raman spectroscopy and scanning transmission electron microscopy," Nano Lett. **15**(9), 5667–5672 (2015).

[20] Lazzeri, M. and Mauri, F., "Nonadiabatic Kohn anomaly in a doped graphene monolayer," Phys. Rev. Lett. **97**(26), 266407 (2006).
[21] Pisana, S., Lazzeri, M., Casiraghi, C., Novoselov, K. S., Geim, A. K., Ferrari, A. C. and Mauri, F., "Breakdown of the adiabatic Born–Oppenheimer approximation in graphene," Nat. Mater. **6**(3), 198–201 (2007).
[22] Yan, J., Zhang, Y., Kim, P. and Pinczuk, A., "Electric field effect tuning of electron-phonon coupling in graphene," Phys. Rev. Lett. **98**(16), 166802 (2007).
[23] Chen, J.-H., Cullen, W. G., Jang, C., Fuhrer, M. S. and Williams, E. D., "Defect scattering in graphene," Phys. Rev. Lett. **102**(23), 236805 (2009).
[24] Lucchese, M. M., Stavale, F., Ferreira, E. H. M., Vilani, C., Moutinho, M. V. O., Capaz, R. B., Achete, C. A. and Jorio, A., "Quantifying ion-induced defects and Raman relaxation length in graphene," Carbon N. Y. **48**(5), 1592–1597 (2010).
[25] Ni, Z. H., Ponomarenko, L. A., Nair, R. R., Yang, R., Anissimova, S., Grigorieva, I. V, Schedin, F., Blake, P., Shen, Z. X., Hill, E. H., Novoselov, K. S. and Geim, A. K., "On resonant scatterers as a factor limiting carrier mobility in graphene," Nano Lett. **10**(10), 3868–3872 (2010).
[26] Rice, C., Young, R. J., Zan, R., Bangert, U., Wolverson, D., Georgiou, T., Jalil, R. and Novoselov, K. S., "Raman-scattering measurements and first-principles calculations of strain-induced phonon shifts in monolayer MoS2," Phys. Rev. B **87**(8), 81307 (2013).
[27] Loudon, R., "Theory of the first-order Raman effect in crystals," Proc. R. Soc. London. Ser. A. Math. Phys. Sci. **275**(1361), 218–232 (1963).
[28] Knight, D. S. and White, W. B., "Characterization of diamond films by Raman spectroscopy," J. Mater. Res. (1989).
[29] Mafra, D. L., Samsonidze, G., Malard, L. M., Elias, D. C., Brant, J. C., Plentz, F., Alves, E. S. and Pimenta, M. A., "Determination of LA and TO phonon dispersion relations of graphene near the Dirac point by double resonance Raman scattering," Phys. Rev. B **76**(23), 233407 (2007).
[30] Fleischmann, M., Hendra, P. J. and McQuillan, A. J., "Raman spectra of pyridine adsorbed at a silver electrode," Chem. Phys. Lett. **26**(2), 163–166 (1974).
[31] Maier, S. A., [Plasmonics: fundamentals and applications], Springer US, New York, NY, MA (2007).
[32] Zheng, X., Volskiy, V., Valev, V. K., Vandenbosch, G. A. E. and Moshchalkov, V. V., "Line Position and Quality Factor of Plasmonic Resonances Beyond the Quasi-Static Limit: A Full-Wave Eigenmode Analysis Route," IEEE J. Sel. Top. Quantum Electron. **19**(3), 4600908 (2013).
[33] Zheng, X., Valev, V. K., Verellen, N., Jeyaram, Y., Silhanek, A. V., Metlushko, V., Ameloot, M., Vandenbosch, G. A. E. and Moshchalkov, V. V., "Volumetric Method of Moments and Conceptual Multilevel Building Blocks for Nanotopologies," IEEE Photonics J. **4**(1), 267–282 (2012).
[34] Patra, P. P., Chikkaraddy, R., Tripathi, R. P. N., Dasgupta, A. and Kumar, G. V. P., "Plasmofluidic single-molecule surface-enhanced Raman scattering from dynamic assembly of plasmonic nanoparticles," Nat. Commun. **5**(1), 4357 (2014).
[35] Kim, T., Lee, K., Gong, M. and Joo, S.-W., "Control of gold nanoparticle aggregates by manipulation of interparticle interaction," Langmuir **21**(21), 9524–9528 (2005).
[36] Taylor, R. W., Lee, T.-C., Scherman, O. A., Esteban, R., Aizpurua, J., Huang, F. M., Baumberg, J. J. and Mahajan, S., "Precise subnanometer plasmonic junctions for SERS within gold nanoparticle assemblies using cucurbit[n]uril 'glue,'" ACS Nano **5**(5), 3878–3887 (2011).
[37] Benz, F., Chikkaraddy, R., Salmon, A., Ohadi, H., De Nijs, B., Mertens, J., Carnegie, C., Bowman, R. W. and Baumberg, J. J., "SERS of individual nanoparticles on a mirror: Size does matter, but so does shape," J. Phys. Chem. Lett. **7**(12), 2264–2269 (2016).
[38] Pieczonka, N. P. W. and Aroca, R. F., "Inherent complexities of trace detection by surface-enhanced Raman scattering," ChemPhysChem **6**(12), 2473–2484 (2005).
[39] Hatab, N. A., Hsueh, C.-H., Gaddis, A. L., Retterer, S. T., Li, J.-H., Eres, G., Zhang, Z. and Gu, B., "Free-standing optical gold bowtie nanoantenna with variable gap size for enhanced Raman spectroscopy," Nano Lett. **10**(12), 4952–4955 (2010).
[40] Kahl, M., Voges, E., Kostrewa, S., Viets, C. and Hill, W., "Periodically structured metallic substrates for SERS," Sensors Actuators B Chem. **51**(1), 285–291 (1998).
[41] Mamonov, E. A., Kolmychek, I. A., Vandendriessche, S., Hojeij, M., Ekinci, Y., Valev, V. K., Verbiest, T. and Murzina, T. V., "Anisotropy versus circular dichroism in second harmonic generation from fourfold symmetric arrays of G-shaped nanostructures," Phys. Rev. B - Condens. Matter Mater. Phys. **89**(12), 1–5 (2014).

[42] Mamonov, E. A., Murzina, T. V., Kolmychek, I. A., Maydykovsky, A. I., Valev, V. K., Silhanek, A. V., Verbiest, T., Moshchalkov, V. V. and Aktsipetrov, O. A., "Chirality in nonlinear-optical response of planar G-shaped nanostructures," Opt. Express **20**(8), 8518 (2012).
[43] Valev, V. K., Kirilyuk, A., Dalla Longa, F., Kohlhepp, J. T., Koopmans, B. and Rasing, T., "Observation of periodic oscillations in magnetization-induced second harmonic generation at the Mn/Co interface," Phys. Rev. B **75**(1), 12401 (2007).
[44] Vincent, B., Loo, R., Vandervorst, W., Delmotte, J., Douhard, B., Valev, V. K., Vanbel, M., Verbiest, T., Rip, J., Brijs, B., Conard, T., Claypool, C., Takeuchi, S., Zaima, S., Mitard, J., De Jaeger, B., Dekoster, J. and Caymax, M., "Si passivation for Ge pMOSFETs: Impact of Si cap growth conditions," Solid. State. Electron. **60**(1), 116–121 (2011).
[45] Xu, G., Cheng, H., Jones, R., Feng, Y., Gong, K., Li, K., Fang, X., Tahir, M. A., Valev, V. K. and Zhang, L., "Surface-Enhanced Raman Spectroscopy Facilitates the Detection of Microplastics <1 μm in the Environment," Environ. Sci. Technol. **54**(24), 15594–15603 (2020).
[46] Tahir, M. A., Zhang, X., Cheng, H., Xu, D., Feng, Y., Sui, G., Fu, H., Valev, V. K., Zhang, L. and Chen, J., "Klarite as a label-free SERS-based assay: a promising approach for atmospheric bioaerosol detection," Analyst **145**(1), 277–285 (2020).
[47] Valev, V. K., Smisdom, N., Silhanek, A. V., De Clercq, B., Gillijns, W., Ameloot, M., Moshchalkov, V. V. and Verbiest, T., "Plasmonic ratchet wheels: Switching circular dichroism by arranging chiral nanostructures," Nano Lett. **9**(11), 3945–3948 (2009).
[48] Smitha, S. L., Gopchandran, K. G., Smijesh, N. and Philip, R., "Size-dependent optical properties of Au nanorods," Prog. Nat. Sci. Mater. Int. **23**(1), 36–43 (2013).
[49] Vrancken, M. and Vandenbosch, G. A. E., "Hybrid dyadic-mixed-potential and combined spectral-space domain integral-equation analysis of quasi-3-D structures in stratified media," IEEE Trans. Microw. Theory Tech. **51**(1), 216–225 (2003).
[50] Schols, Y. and Vandenbosch, G. A. E., "Separation of horizontal and vertical dependencies in a surface/volume integral equation approach to model quasi 3-D structures in multilayered media," IEEE Trans. Antennas Propag. **55**(4), 1086–1094 (2007).
[51] "Lumerical Solutions, inc.", <http://www.lumerical.com/>.
[52] Oskooi, A. F., Roundy, D., Ibanescu, M., Bermel, P., Joannopoulos, J. D. and Johnson, S. G., "Meep: A flexible free-software package for electromagnetic simulations by the FDTD method," Comput. Phys. Commun. **181**(3), 687–702 (2010).
[53] "Diffract MOD, RSoft Design Group.", <http://www.rsoftdesign.com>.
[54] Palik, E., [Handbook of Optical Constants of Solids], Academic Press (1998).
[55] Lide, D. R., [CRC handbook of chemistry and physics], CRC press (2004).
[56] Madzharova, F., Heiner, Z., Simke, J., Selve, S. and Kneipp, J., "Gold Nanostructures for Plasmonic Enhancement of Hyper-Raman Scattering," J. Phys. Chem. C **122**(5), 2931–2940 (2018).
[57] Gühlke, M., Heiner, Z. and Kneipp, J., "Surface-enhanced hyper-Raman and Raman hyperspectral mapping," Phys. Chem. Chem. Phys. **18**(21), 14228–14233 (2016).
[58] Kuppe, C., Zheng, X., Williams, C., Murphy, A. W. A., Collins, J. T., Gordeev, S. N., Vandenbosch, G. A. E. and Valev, V. K., "Measuring optical activity in the far-field from a racemic nanomaterial: Diffraction spectroscopy from plasmonic nanogratings," Nanoscale Horizons **4**(5), 1056–1062 (2019).
[59] Hakonen, A., Andersson, P. O., Stenbæk Schmidt, M., Rindzevicius, T. and Käll, M., "Explosive and chemical threat detection by surface-enhanced Raman scattering: A review," Anal. Chim. Acta **893**, 1–13 (2015).
[60] Xu, L. J., Lei, Z. C., Li, J., Zong, C., Yang, C. J. and Ren, B., "Label-free surface-enhanced Raman spectroscopy detection of DNA with single-base sensitivity," J. Am. Chem. Soc. (2015).
[61] Shanmukh, S., Jones, L., Driskell, J., Zhao, Y., Dluhy, R. and Tripp, R. A., "Rapid and sensitive detection of respiratory virus molecular signatures using a silver nanorod array SERS substrate," Nano Lett. **6**(11), 2630–2636 (2006).